Medical Image Analysis 16 (2012) 662–674

Contents lists available at ScienceDirect

Medical Image Analysis

journal homepage: www.elsevier.com/locate/media

Biomechanically constrained groupwise ultrasound to CT registration of the lumbar spine

Sean Gill [a], Purang Abolmaesumi [a,b], Gabor Fichtinger [a], Jonathan Boisvert [c], David Pichora [d], Dan Borshneck [d], Parvin Mousavi [a,*]

[a] Queen's University, Kingston, ON, Canada
[b] University of British Columbia, Vancouver, BC, Canada
[c] Institute for Information Technology, National Research Council Canada, Ottawa, ON, Canada
[d] Kingston General Hospital, Kingston, ON, Canada

ARTICLE INFO

Article history:
Received 11 September 2009
Received in revised form 28 February 2010
Accepted 11 July 2010
Available online 4 August 2010

Keywords:
Ultrasound
Spine
Multimodal registration
Biomechanical model

ABSTRACT

We present a groupwise US to CT registration algorithm for guiding percutaneous spinal interventions. In addition, we introduce a comprehensive validation scheme that accounts for changes in the curvature of the spine between preoperative and intraoperative imaging. In our registration methodology, each vertebra in CT is treated as a sub-volume and transformed individually. A biomechanical model is used to constrain the displacement of the vertebrae relative to one another. The sub-volumes are then reconstructed into a single volume. During each iteration of registration, an US image is simulated from the reconstructed CT volume and an intensity-based similarity metric is calculated with the real US image. Validation studies are performed on CT and US images from a sheep cadaver, five patient-based phantoms designed to preserve realistic curvatures of the spine and a sixth patient-based phantom where the curvature of the spine is changed between preoperative and intraoperative imaging.

For datasets where the spine curve between two imaging modalities was artificially perturbed, the proposed methodology was able to register initial misalignments of up to 20 mm with a success rate of 95%. For the phantom with a physical change in the curvature of the spine introduced between the US and CT datasets, the registration success rate was 98.5%. Finally, the registration success rate for the sheep cadaver with soft-tissue information was 87%. The results demonstrate that our algorithm allows for robust registration of US and CT datasets, regardless of a change in the patients pose between preoperative and intraoperative image acquisitions.

1. Introduction

In 2002, almost two-thirds of Canadian adults reported at least a mild level of back pain, leading to approximately $16.4 billion lost to the cost of treatment and lost productivity (Environics Research Group Limited, 2003). In the United States, this cost has been reported as $62 billion (Allen et al., 2005; Stewart et al., 2003). Oral medication is the standard primary method of treatment, however Raj et al. (2003) found that 21% of patients reported no improvement and nearly half the patients surveyed reported little improvement in back pain. More recently, improved results for oral medication have been reported (Mahowald et al., 2005), however for many patients, it is simply not an effective form of treatment. For such patients, the next step is spinal injections. These percutaneous interventions involve inserting a needle through the skin into the targeted tissue region, in this case the facet joint. A local anaesthetic and steroid are then injected to reduce pain and inflammation. Spinal injections for back pain management are frequently carried out in hospitals and radiological clinics. Currently, these procedures are performed under fluoroscopy or computed tomography (CT) guidance. Intraoperative CT and fluoroscopy can provide detailed images of the patient anatomy and needle location throughout the procedure. However, in order to use CT or fluoroscopic guidance, the procedure has to be performed in specialized interventional radiological facilities, thus imposing a major financial burden on the healthcare system. Another drawback with the current practice is patient and surgeon exposure to X-ray radiation. In CT-guided procedures, a minimum of three scans are required for identifying the needle target, rescanning the patient with a fiducial marker placed in the target plane and confirming an acceptable insertion. This number can increase for more difficult cases, such as scoliotic patients. A typical intervention can take between 10 and 45 min, depending on the experience of the physician and complications that arise. A significant portion of this time can be attributed to the medical staff needing to leave

* Corresponding author.
E-mail address: pmousavi@cs.queensu.ca (P. Mousavi).

1361-8415/$ - see front matter © 2010 Elsevier B.V. All rights reserved.
doi:10.1016/j.media.2010.07.008

the room when an image is acquired. The work presented here is part of a larger effort to develop an US-guided percutaneous spinal intervention system and eliminate the need for intraoperative X-ray-based imaging. Additionally, an US-guided intervention system would allow the procedure to be performed in a neurosurgeon's office, eliminating the use of expensive specialized facilities and reducing the wait time and travel for patients.

Galiano et al. (2005) performed a cadaver study using US as the guidance modality for facet joint injections and successfully inserted the needle tip into the targeting tissue region. While, US imaging is portable and inexpensive with no known side effects, the use of US as a sole guidance modality introduces its own challenges. US images are acquired from the propagation of sound waves through tissue. The transmission and reflection of the signal is dependent on the interaction of the signal at inhomogeneous tissue interfaces. One of the major factors in this interaction is the density of the tissue. The transition from soft to bony tissue, a large change in density, often causes full reflection of the US signal. This occludes any anatomy below the bony and soft-tissue interface, making it impossible to visualize in the US image. Due to the significant reflection occurring at these interfaces, the surface of the bony structure appears bright in the image, but is often blurred and difficult to identify exactly. Additionally, not all bone surfaces are visible in US. If an US signal reflects at a bony and soft-tissue interface that is angled away from the US transducer, the signal will not return to the transducer and the surface will not appear in the US image. Finally, US images contain significant noise in the soft-tissue portion of the image. US as a sole modality for guidance is not ideal, as a clear depiction of the location of the needle relative to the target anatomy is essential for a clinically viable guidance system.

It is common for patients who require a percutaneous spinal intervention for pain relief to have a CT image acquired as a diagnostic step. This CT would contain information on the shape and structure of the spine, including anatomy not visible in US. Therefore, this work considers the fusion of intraoperative US with preoperative CT for guiding percutaneous spinal injections. Fig. 1 shows an example of corresponding anatomy in slices from US and CT and an overlay displaying the CT bone edges in US space.

The use of a preoperative CT image introduces an additional challenge to the fusion of US and CT. In order to minimize motion artefacts, the preoperative CT is acquired with the patient in a supine position. Conversely, the intervention is performed with the patient prone. Thus, the intraoperative US image will be of the patient in the prone position, introducing a change in the curvature of the spine across the US and CT datasets. The registration of the US and CT data will need to account for any change in the curvature of the spine caused by the change in pose.

Much of the early work in US to CT registration of boney structures was centered on feature-based registration. Surfaces would be extracted from the US and CT and registered using Iterative Closest Point (ICP) (Besl and McKay, 1992) and its variations. One common issue in these feature-based registrations is the need to extract surface information from US. US images are noisy and only display portions of the bone surface; this makes automatic segmentation of the bone surface difficult to accomplish and manual segmentation cumbersome to reproduce accurately. An additional issue with the use of ICP is the need for a sufficiently accurate initial alignment.

Working with cadaveric and clinical data for the placement of iliosacral screws, Carrat et al. (2000) and Tonetti et al. (2001) manually extracted bone surfaces from US, which were subsequently registered to CT images of the sacrum using ICP. While no quantitative errors for the registration process was calculated, screw placement was found to improve under the use of the system. Herring et al. (1998) collected US images of a plastic spine phantom submerged in water and automatically extracted surface points using a combination of morphological operations and ray tracing. Using ICP to register this set of points to an extracted CT surface produced promising results; however, in this preliminary work they lacked a system to track the US probe and so the results were not quantitatively verified. Muratore et al. (2002) collected tracked US and CT data of a plastic spine phantom submerged in water. Surfaces were extracted automatically, using a modified marching cubes algorithm for CT and a similar extraction approach to Herring et al. (1998) for US. Using ICP, registration was performed for each vertebra sequentially, with errors below 2 mm. A plastic model submerged in a water bath produces cleaner US images than would be found clinically, making extraction of the bone surface easier. While the authors show a visual extraction of bone surface in a human US image, no quantitative results were presented. Amin et al. (2003) performed an ICP registration on US and CT data collected from a pelvic phantom submerged in water and from intraoperative patient data. Their approach differs from prior work in that 2D regions that are likely to be bone surfaces are extracted from the US data. During ICP registration, pixels in these regions are weighted according to their proximity to the initial estimate of the registration, the intensity of the pixels and the shadow region beyond the pixels. In phantom tests, translation error was below 1 mm and 1° along each axis. When comparing this registration technique to registration of physically acquired points on intraoperative patient data, an average difference of less than 2 mm and 1° along each axis was found. No absolute errors for patient data were reported though. This approach puts further emphasis on the initial alignment of the datasets due to the weighting of the ICP registration according to the initial pixel proximity of US to the CT surface. More recent work has focused on eliminating errors within the registration optimization procedure. Barratt et al. (2005) presented a method for concurrent registration and calibration of the US probe *in vivo* based on segmented US and CT surfaces. The optimization scheme minimizes the distance between surface points, but used the iterative region

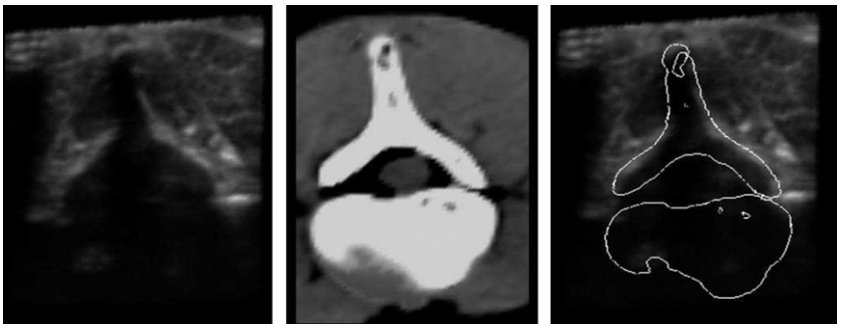

Fig. 1. Transverse slice from an US volume (left); the corresponding CT slice (center); and an overlay of the CT bone contours with the US slice (right) in a sheep cadaver.

trust optimization scheme in place of ICP. Updating the calibration throughout the registration produced less error compared to previous registration techniques. However, the published implementation used manually segmented US surfaces. Additionally, this work was tested on data from the pelvis and femur, which produce significantly different US images from those of the spine. Similarly, Moghari and Abolmaesumi (2005) improved upon the registration process with the implementation of an Unscented Kalman Filter replacing the ICP algorithm. This approach was only reported for manually extracted US points. While they improved on feature-based registrations of US to CT images, they are still reliant on extraction of bone surface points from US, which is difficult to reproduce and not robust for automatic implementation.

Intensity-based registration eliminates the need for segmentation of bone surfaces and allows for the inclusion of information in the images that would otherwise be discarded in feature-based registrations. Winter et al. (2008) based their registration algorithm on the fact that the brightest points in US images are most often caused by the reflection of the signal on the bone surface. After extracting the bone surface from the CT volume, the surface is degraded to only what is expected to be visible in US. This degraded surface is then registered to the US volume, maximizing the overlapping greyscale value. While this approach eliminates the need to extract the bone surface from US, the degradation of the CT surface requires prior knowledge of the orientation of the US probe when it scans the tissue. Shao et al. (2006) presented a similar approach in registering transrectal US to MR images of the pubic arch, where the bone surface is extracted from MR and registered to the US volume. Three similarity measures were compared in this work: maximizing overlapping intensity in US, maximizing the gradient in US and maximizing the image intensity while minimizing the intensities of the region below the surface. The inclusion of shadow information was found to significantly improve the registration results. This approach still required prior knowledge of the probe orientation. Standard intensity-based approaches assume a mapping between the two modalities. This assumption fails in US images as the intensity is not solely based on the tissue properties, particularly in images with significant occlusion due to bony and soft-tissue interfaces. For this reason, preprocessing has been attempted to make intensity-based registration possible. Working with an abdominal phantom, von Berg et al. (2004) applied preprocessing to the CT image to bring it closer to the US image. Bone edges were identified and any regions beyond were masked using a ray casting approach. This approach introduces a possible source of error: if the assumed beam direction is incorrect, it will decrease the similarity of the images. The authors tested both Normalized Mutual Information (NMI) and Cross-Correlation (CC) as similarity metrics. Results were only reported for 2D to 3D and in-plane registration, and resulting errors were above what would be acceptable for most percutaneous spinal interventions. Huang et al. (2006) presented a similar method, designed to register US and CT images of the rib cage as a form of initialization for US to MR registration of the heart. The US images were preprocessed to remove the background noise with a threshold filter. For CT preprocessing, a morphological operator and gradient based threshold filter were applied to eliminate bone edges that would not be visible in US. As the registration technique was tested on a phantom submerged in water, the US images remained cleaner than clinical images would have been. Like previous work, this approach also requires prior knowledge of the US scan direction. Penney et al. (2006) presented a novel approach for registration of the pelvis and femur where both the US and CT images are converted to intermediate images that are then registered together. In this work, each voxel in both US and CT is given a probability of being a bony edge. In CT, features for each voxel are extracted for the current intensity and the maximum intensity within a region around the voxel. In US, the features are identified as the current voxel intensity and the number of voxels that are not identified as shadow below the current voxel. The probability of a voxel with a given set of features is determined by the number of voxels identified to be a bone edge with the same set of features. While this approach produces accurate registrations, for clinically relevant probabilities, a large set of prior CT and US images would have to be manually segmented and would be dependent on the region being registered.

A recent approach for intensity-based registration focused on US simulation from CT that is updated throughout the registration. Wein et al. (2005) first presented this approach for a rigid US to CT registration of the head and neck. The algorithm extracts slices from the CT volume that correspond to the scan plane of the US probe. These CT slices are then processed to extract edge information and used to calculate a weighted MI similarity metric composed of several components, including skin clamping and edge alignment. The algorithm limits the registration region of interest to non-occluded areas within the CT slices. In continuing work Wein et al. (2007, 2008) presented a method that simulates US reflection from the CT data based on US signal propagation. This is then combined with a CT volume with intensities mapped closer to US values. By updating this combination of images at each iteration of the registration, the algorithm is able to optimize the simulation as the registration proceeds. This work was presented for registration of the liver and was found to be more robust and accurate than directly registering the images with either MI or CC. This algorithm was extended by Shams et al. (2008) to create a more realistic simulation for training physicians and technicians in the use of US imaging. This technique requires preprocessing to create a scatter volume of the CT data using the Field II US simulator (Jensen and Svendsen, 1992, 1996), which remains time consuming and makes this approach less appropriate for intraoperative registrations. Reichl et al. (2009) and Kutter et al. (2009) presented an iterative US simulation and registration implemented in GPU, resulting in significantly decreased algorithm run time. Previously, we (Gill et al., 2009b) proposed an extension of the work from Wein et al. (2007, 2008), focusing on bone-based registration and introduced a groupwise US to CT registration of the lumbar spine in a phantom of L3, L4 and L5. This algorithm allows free motion of the vertebrae and registers all three simultaneously. We further extended this work by introducing a biomechanical model to constrain the motion of the vertebra, in order to maintain clinically realistic orientations (Gill et al., 2009a). Kadoury and Paragios (2009) presented an alternate method to registering an articulated spine model to intraoperative patient CT data. A preoperative spine model of 17 vertebrae (T1–T12 and L1–L5) is registered to the intraoperative data using Markov Random Fields (MRF) as the optimization scheme. In this approach, the interactions between vertebrae are not assumed, but are optimized as part of the registration. This approach takes into account both an intensity-based measure and a pairwise measure determined by the alignment of the vertebrae relative to their original pose. The approach, however, does not take into account the fact that motion along some axes is more difficult than others and therefore is less likely to occur.

We present a comprehensive validation of our biomechanically constrained US to CT registration of the spine (Gill et al., 2009a). This algorithm initially rigidly registers the US and CT data using our US simulation from CT technique. In this work, the US simulation has been modified to emphasize the soft-tissue–bone interface. Following the rigid initialization, each vertebra is simultaneously rigidly registered to the US volume. This step is performed to account for changes in the curvature of the spine between the preoperative and intraoperative imaging. A biomechanical model is used to constrain the motion of the vertebrae relative to one another.

The registration technique is validated on data from patient-based phantoms and a sheep cadaver. The target area for a facet joint injection is approximately 1.5 cm in diameter. Given the size of the target, we expect that an accuracy of 3 mm should be sufficient for the approach to be clinically acceptable. The patient-based phantoms have been designed to preserve a realistic representation of the curvature of the spine. Registration is performed on vertebrae L2, L3 and L4 for both rigid and groupwise tests. In the patient-based phantom groupwise tests, the curvature of the spine is altered between US and CT datasets. This is done using two approaches: artificially changing the curvature in CT by applying different initial transforms to each vertebra, and manually altering the curvature of the spine model between the CT and US data collection. Rigid and groupwise registration tests are performed on the sheep cadaver, with the curvature of the spine artificially changed for the groupwise tests. Registration error and success rates are reported for both the rigid and groupwise algorithms across all datasets. Finally, we discuss the strengths of this registration technique, possible sources of error and our future plans for this work.

2. Method

In this section we present our proposed US to CT registration technique and we detail the biomechanical model used to constrain the groupwise registration. Our registration technique iteratively simulates an US image at each step of the registration. This is performed in three stages: (1) an US signal is simulated passing through the tissue to produce a map of the reflections from the tissue interfaces, (2) the intensities in the CT volume are mapped to corresponding values found in US and finally, (3) these two intermediate images are weighted and combined to best match the current overlapping US voxels. The simulated US is updated iteratively throughout the registration. Our similarity metric, based on Correlation Ratio (CR), is calculated by comparing the US volume with the simulated US volume.

A rigid registration optimizes a single set of six parameters (three rotations, three translations) for the entire volume. This is used to initially align the US and CT data. To account for changes in the curvature of the spine between the preoperative and intraoperative imaging, the groupwise registration treats each vertebra in CT as an independent rigid body and registers them simultaneously to the US volume. This results in an optimization of $n \times 6$ parameters, where n is the number of vertebrae registered to the US. Finally, to improve the groupwise registration accuracy and restrict the registration to biologically realistic alignments, a biomechanical model is introduced to constrain the orientation of vertebrae relative to one another.

2.1. Rigid registration and US simulation

The workflow for the US simulation and registration is shown in Fig. 2. The six degrees-of-freedom are represented by an Euler transform. Covariant Matrix Adaption Evolution Strategy (CMA-ES) (Hansen et al., 2003) is used as the optimization strategy. CMA-ES was chosen because in our previous work (Gill et al., 2009b) we found it to be robust for US to CT simulation and registration when compared with Gradient Descent and Simplex optimization schemes.

The simulation of ultrasound reflections models the ultrasound beam passing through the tissue as a ray. An assumption is made that the CT intensities (in Hounsfield units) can be related to the acoustic impedance values used to calculate ultrasound transmission and reflection. The simulated beam passes through each column of the volume. The transmission and reflection of the beam is calculated at each voxel according to the following equations originally presented by Wein et al. (2007, 2008),

$$\Delta r(x,y,d) = (d^T \nabla \mu(x,y)) \frac{|\nabla \mu(x,y)|}{(2\mu(x,y))}, \tag{1}$$

$$\Delta t(x,y) = 1 - \left(\frac{|\nabla \mu(x,y)|}{(2\mu(x,y))} \right)^2, \tag{2}$$

$$r(x,y) = I(x,y-1)\Delta r(x,y,d), \tag{3}$$

$$I(x,y) = \begin{cases} I(x,y-1)\Delta t(x,y), & |\nabla \mu(x,y)| < \tau, \\ 0, & |\nabla \mu(x,y)| \geqslant \tau, \end{cases} \tag{4}$$

where d is the direction of the US beam, μ is the intensity of the CT image, Δr is the reflection coefficient, r is the simulated reflection intensity, Δt is the transmission coefficient, τ is the threshold for full reflection and I is the intensity of our simulated US beam. Eq. (4) has been modified such that any gradient value greater than a set threshold causes full reflection of the US beam intensity at that point, setting the incoming US beam intensity for all subsequent points on the scan line to zero. The value of our threshold was set to 250 Hounsfield units. We compared many values across our phantoms, sheep cadaver and patient datasets and found this value to best capture true bone edges, while minimizing the number of false bone edges produced. Voxels where full reflection occurs are flagged as a bone–soft-tissue interface. At any point in the simulation, if the intensity of the simulated US beam reaches zero, due to gradual reduction of beam intensity or from full reflection, the remaining voxels along the scan line are flagged as occluded. A log-compression is applied to the simulated reflection image to amplify small reflections,

$$r(x,y) = \frac{\log(1 + ar(x,y))}{\log(1+a)}, \tag{5}$$

where a is a user-defined value.

Reflections from tissue interfaces only comprise a portion of the US image. To include further tissue information, the CT intensities are mapped to values closer to those corresponding to the tissues in the US data, using an approximation of the curve presented in Wein et al. (2007, 2008),

$$p(x,y) = 1.36\mu(x,y) - 1429. \tag{6}$$

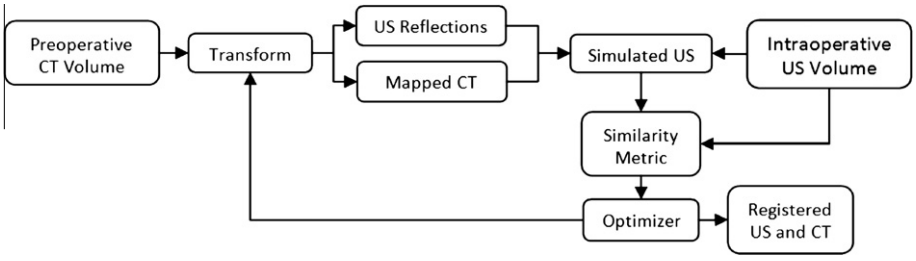

Fig. 2. Workflow of the rigid US to CT simulation and registration.

The final step of the US simulation is to compute weight values for the simulated US reflection, the mapped CT and the bias term. The bias term can be thought of as an averaged intensity value of the US soft-tissue region. At each voxel, the weighted simulated US reflection and mapped CT are added to this averaged intensity to produce the final simulated US intensity. A least-squares optimization is used to compute the weights and bias term, such that the difference between the final simulated US and real US intensities is minimized across all overlapping voxels. This is done in the same manner as the weight calculation presented by Wein et al. (2007, 2008) however, we do not include any voxels that are identified as occluded in the simulation as part of the weight calculation. The overlap between the US and CT images, as well as the US voxels identified as occluded will vary at each iteration. This in turn causes the values of the weights, the bias term and ψ to vary at each iteration of the optimization. Occluded voxels are treated as a separate region within the image. The intensity value of occluded voxels in US is dependent on many factors, and can vary between datasets. However, we know that the occluded voxels have approximately the same intensity in any given scan. As such, we set the value of all occluded voxels in the simulation to be the mean of the intensity values in the US that overlap the occluded region. The final simulation is calculated in the same manner as the work presented by Wein et al. (2007, 2008), with an additional case for occluded voxels. The final simulation is calculated as,

$$f(x,y) = \begin{cases} \alpha_i p(x,y) + \beta_i r(x,y) + \gamma_i, & I(x,y) > 0, \\ \psi, & I(x,y) = 0, \end{cases} \tag{7}$$

where f is the simulated US image, α, β are the weights, γ is the bias term and ψ is the mean US intensity from voxels overlapping the occluded voxels in the simulation. Additionally, any voxels that are flagged as a bone–soft-tissue interface are set to the maximum value found in the US dataset. This forces the interface to remain bright in the simulation, regardless of what voxels it overlaps in the US. An example of the simulated US is shown in Fig. 3.

Similarity between the real US image and the simulated US image is calculated using the Linear Correlation of Linear Combination (LC^2) metric used by Wein et al. (2007, 2008),

$$LC^2 = \frac{\sum (U(x,y) - f(x,y))^2}{N \times Var(U)}, \tag{8}$$

where N is the number of overlapping voxels between the US and CT images, and U is the real ultrasound image intensity. All voxels, including occluded voxels, are used in the calculation of the similarity metric.

2.2. Groupwise registration

In a clinical setting, the preoperative CT of the patient will be acquired in the supine position, while the intervention will be performed with the patient in the prone position. This introduces a change in the curvature of the spine which must be accounted for in the registration process. We propose a groupwise registration that treats each vertebra as a distinct rigid body that moves separately and registers all vertebrae simultaneously.

A rigid registration is performed over the entire US and CT volumes to determine the initial alignment for the subsequent groupwise registration. The rigid registration provides a global alignment for the US and CT volumes, while the groupwise registration allows for the registration of any discrepancies in the orientation of the vertebrae between the volumes. For the groupwise algorithm, the CT volume is initially cut into sub-volumes, each containing a single vertebra. Voxels in the sub-volumes corresponding to bone from an adjacent vertebra were masked. The registration treats each vertebra independently, allowing for six degrees-of-freedom. All vertebrae are registered simultaneously,

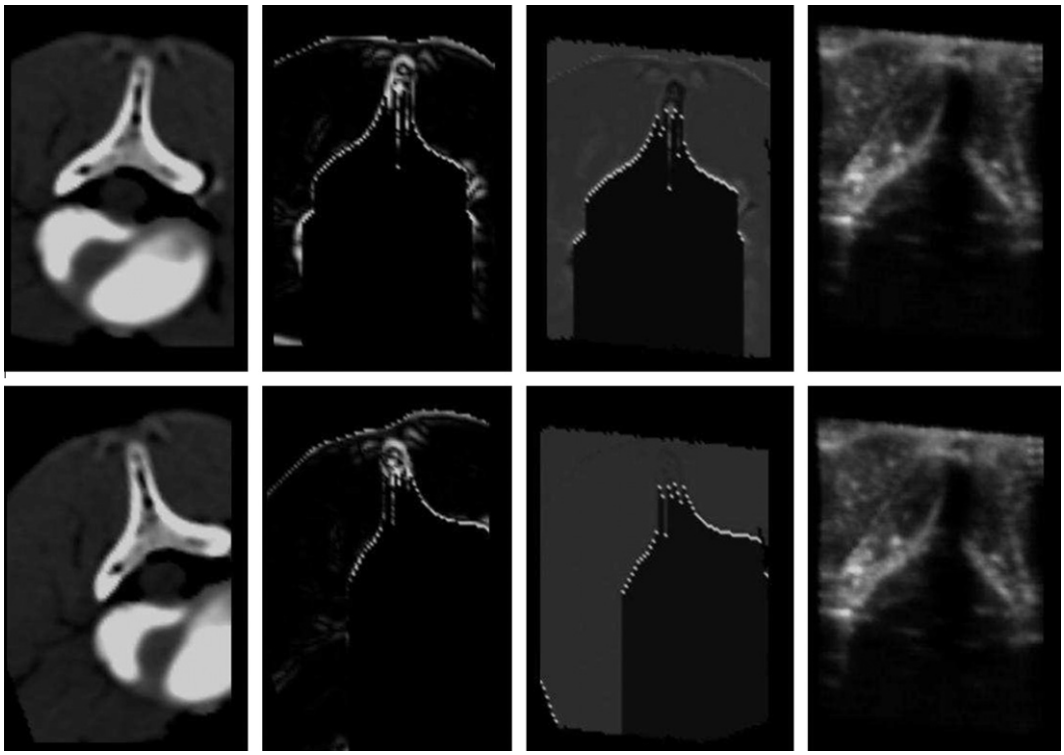

Fig. 3. Transverse slices from registered (top) and misaligned (bottom) datasets, including CT (left), simulated US Reflections (center left), simulated US (center right) and US (right). The difference in the occluded region in the simulated US reflections and the decreased clarity of soft-tissue in the simulated US can be seen when comparing the misaligned and registered intermediate images.

resulting in an optimization with $n \times 6$ parameters, where n is the number of vertebrae being registered. After the transformations are applied, the sub-volumes are reconstructed into a single volume. Bony structures are preserved by setting the reconstructed value to the maximum intensity of any overlapping voxels. Any gaps in the final volume are filled with a default value approximating the intensity of soft-tissue in the CT. The US simulation is applied to this reconstructed volume and the similarity metric is calculated between the resulting simulated US volume and the actual US volume.

2.3. Biomechanical model

Allowing free motion of vertebrae during registration is not ideal as it does not distinguish between anatomically realistic orientations of vertebrae and orientations where the vertebrae are colliding, unreasonably oriented or far apart. A biomechanical model of the spine can constrain the registration and favour anatomically acceptable alignments. The final workflow of our groupwise registration is modified to include the biomechanical model as shown in Fig. 4.

The biomechanical model used is from the work of Desroches et al. (2007) which in turn was adapted from previously published data from Panjabi et al. (1976) and Gardner-Morse et al. (1990). Panjabi et al. (1976) calculated three-dimensional load–displacement curves to model the motion of the vertebrae by applying force and torque to cadaveric vertebrae and measuring their displacement. The model used represents the relation between the displacement of the intervertebral structures, as well as the reaction forces (F_s) and moments (M_s).

$$\begin{bmatrix} F_x \\ F_y \\ F_z \\ M_x \\ M_y \\ M_z \end{bmatrix} = \begin{bmatrix} 100 & 0 & 50 & 0 & -1640 & 0 \\ 0 & 110 & 0 & 150 & 0 & 580 \\ 50 & 0 & 780 & 0 & -760 & 0 \\ 0 & 150 & 0 & 1.48E5 & 0 & -8040 \\ -1640 & 0 & -760 & 0 & 1.52E5 & 0 \\ 0 & 580 & 0 & -8040 & 0 & 1.53E5 \end{bmatrix} \begin{bmatrix} T_x \\ T_y \\ T_z \\ R_x \\ R_y \\ R_z \end{bmatrix}, \tag{9}$$

where T_s and R_s are the translation and rotation of the vertebrae along a given axis. We define the 6×6 stiffness matrix representing the intervertebral structures as K. The vector of translations (T_x, T_y, T_z) and rotations (R_x, R_y, R_z) we define as x. For our case, x is calculated as the relative transform between two consecutive vertebrae, represented as translation in millimetres along each axis and rotation in radians about each axis. Each vertebra is expected to have no change in rotational orientation and no translation along the transverse and sagittal axes. The expected translation along the coronal axis is defined as the distance between the centers of consecutive vertebrae in the patient's US data. This can be difficult to measure exactly; however it is meant only as an approximation of the vertebral resting position.

The energy of the system is calculated using the general spring equation,

$$U = \frac{1}{2}(x^T K x). \tag{10}$$

The energy is calculated across all vertebrae and normalized based on the energy of a maximum misalignment (10 mm translation along each axis and 10° rotation about each axis),

$$E = \frac{\sum_{i \in V}^{V} U_{\mathrm{Li,Li+1}}}{|V| \times U_{max}} \tag{11}$$

where E is the normalized energy of the system, V is the set of vertebrae to be registered, $U_{\mathrm{Li,Li+1}}$ represent the energy of the model calculated for adjacent vertebrae, and U_{max} is the energy of the maximum misalignment.

This normalized energy is then combined with the LC^2 metric to give the Biomechanically Constrained Linear Correlation of Linear Combination ($BCLC^2$),

$$BCLC^2 = LC^2 - \sigma E, \tag{12}$$

where σ is a user-defined weight used to blend the biomechanical model measure with the LC^2 intensity-based measure. In our work σ was tested at values of 0, 0.5, 1 and 2. This treats the energy of the biomechanical model as a penalty to the intensity-based similarity metric. The optimizer will attempt to minimize the energy of the system while maximizing the intensity-based measure, encouraging biologically realistic solutions.

3. Experiments and results

Registration and validation were performed on patient-based phantoms of the lumbar spine, a curved patient-based phantom and on a sheep cadaver (Fig. 5). Sheep was chosen as it has been found to have a sufficiently realistic approximation of the human spine, particularly in the thoracic and lumbar area (Wilke et al., 1997).

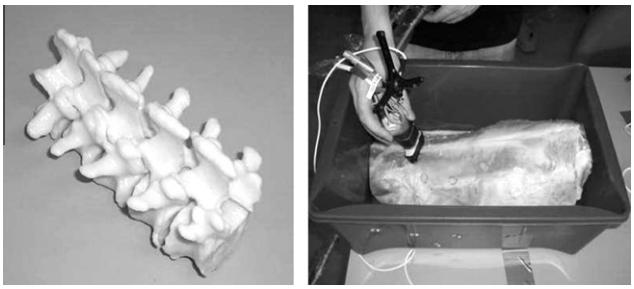

Fig. 5. The patient-based lumbar spine model, prior to being placed in a tissue phantom (left) and the lamb cadaver used in our experiments (right).

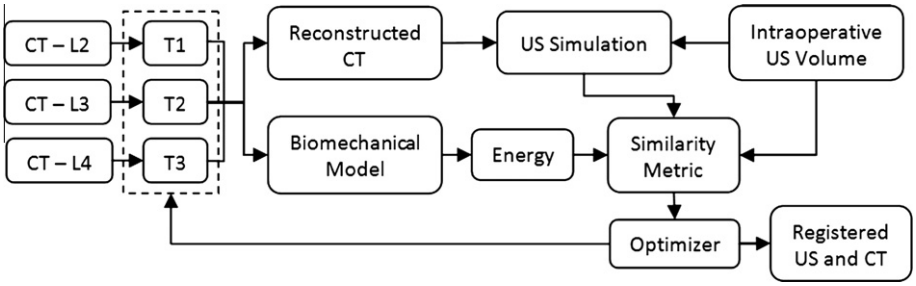

Fig. 4. Workflow of the biomechanically constrained groupwise US to CT simulation and registration. The transforms in this workflow are initialized by a rigid registration.

A high-resolution CT volume and an US volume were acquired from each test subject. The CT volumes for the phantoms were captured at 0.46 mm × 0.46 mm × 0.625 mm, while the resolution of the CT scan for the sheep cadaver was slightly lower at 0.70 mm × 0.70 mm × 0.625 mm. The US volume was reconstructed from a freehand sweep using an L14-5/38 linear-array transducer and a Sonix RP ultrasound machine (Ultrasonix, Richmond, BC, Canada) operating at 6.6 MHz with a depth of 5.5 cm. The probe was tracked using an Optotrack Certus System (Northern Digital Inc., Waterloo, ON, Canada) and calibrated using an N-wire US phantom (Chen et al., 2008). All registrations were performed on a Dell Precision 690, with 2 × 2.33 GHz Intel Xeon Quad-core CPU and 16 GB of RAM.

Through our registration tests of the patient-based phantoms, the curved patient-based phantom and the sheep cadaver, we will show our registration to be robust to a variety of challenges that are presented in a clinical case. The rigid registration of the patient-based phantoms will show that our algorithm can accurately register US and CT datasets containing significant occlusion due to bony and soft-tissue interfaces. The groupwise registration tests for the patient-based phantom will demonstrate that changes in the curvature of the spine can be robustly accounted for through the use of a biomechanical model constraining the motion of the vertebrae throughout the registration optimization. The curved phantom experiments show that this will hold true not only for artificially misaligned datasets, but for US and CT data where a change in curvature has been introduced between preoperative and intraoperative imaging. Finally, in the registration of the sheep cadaver data, we will show the algorithm to be robust to the addition of soft-tissue structures in the US and CT images.

3.1. Patient-based phantoms

Vertebrae L1 to L5 were manually segmented from five patient CT datasets, using ITK-SNAP[1]. The contour lines were converted to a surface model and the spine was printed using a Cimetrix 3D shape printer (Cimetrix Solutions, Oshawa, ON, Canada). This approach preserves both the shape of the vertebrae and the natural curvature of the spine between the patient CT and the printed spine model. The model was placed in a box and was filled with an agar–gelatine mixture based on the recipe presented by Madsen et al. (2005). This recipe was designed to simulate the appearance of soft-tissue in US, including speckle and refraction. The CT and US data of the tissue phantoms were aligned to the gold standard, determined by fiducial markers placed on the exterior of the phantom box. Ten fiducial markers used for calculating the gold standard were placed on the outside of the box. The fiducials surrounded the vertebrae, to maximize the accuracy of ground truth. The positions of these markers were determined manually in CT. To find the location of the markers relative to the US data, a tracked stylus was used to identify the tip of each fiducial.

3.1.1. Rigid registration

The registration was performed on vertebrae L2, L3 and L4. One hundred registrations of the CT and US data were performed on the data with initial misalignment ranging from 0 mm to 20 mm Target Registration Error (TRE). After aligning the CT and US volumes using the fiducial-based gold standard transform, the CT volume was misaligned by a random transformation chosen from a uniform distribution of ±10 mm translation along each axis and ±10° rotation about each axis. The misaligned CT volumes were then registered back to the US volume using our registration algorithm. Accuracy was determined by the ability of the registration to recover the gold standard alignment. TRE is calculated from the errors of the corners of the bounding box for each vertebra after registration. A registration is considered failed if any of the three vertebrae have a final TRE greater than the clinically acceptable error. The anatomical target of a facet joint injection is approximately 1.5 cm in diameter. The maximum error for a clinically acceptable registration is 3 mm. The results of the rigid registration for the patient-based phantoms are shown in Table 1. Successful registrations are defined as any registration with a final TRE of less than 3 mm. The registration algorithm was successful for 98.8% of the tests across all phantoms, with a mean TRE of 1.44 mm in the successful cases. An example of an initial misalignment and final registration is presented in Fig. 6.

The mean registration runtime across all datasets with the C++/Insight Tool Kit (ITK) implementation was 14 min. When implemented in GPU, the runtime was less than 11 s. These results represent a best case scenario, as the curvature of the spine in US and CT data exactly match. This is unlikely to be the case in a clinical setting. To test the rigid registration accuracy on data that does not exactly match, we performed 100 rigid registrations, where

Table 1
Final TRE for the rigidly registered CT volumes from the patient-based phantoms are presented for vertebrae L2–L4 for all successful registrations. The initial TRE is reported for the successful registration with the largest mean initial error across all three vertebrae. Success rate (SR) is defined as the percentage of registrations where all vertebrae have a final TRE of less than 3 mm.

Phantom	L2 (mm/std)	L3 (mm/std)	L4 (mm/std)	Max iTRE (mm)	SR (%)
1	0.95/0.13	0.80/0.09	0.66/0.08	19.57	99.0
2	0.94/0.08	0.83/0.08	0.80/0.08	19.43	98.0
3	1.07/0.05	0.87/0.04	0.76/0.04	19.60	100.0
4	1.36/0.09	1.47/0.06	1.57/0.09	19.73	100.0
5	1.05/0.05	1.36/0.05	1.65/0.08	19.65	100.0

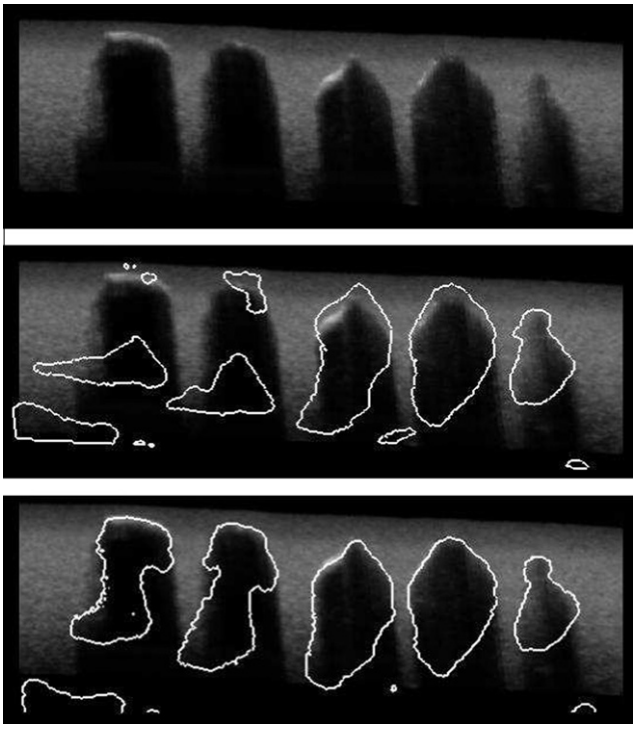

Fig. 6. Sagittal US slice of patient-based phantom 1 (top) overlaid with bone contours from the initially misaligned CT volume (middle) and registered CT volume (bottom).

[1] http://www.itksnap.org

prior to registration the vertebrae were perturbed in CT to produce a different alignment than that found in US. Each vertebra was misaligned by individually applying a random transformation using a uniform distribution of ±5 mm translation along each axis and ±5° rotation about each axis. The volumes were then reconstructed, filling in any gaps with a simulated soft-tissue value. This CT volume was then misaligned by the same set of transformations used in the previous rigid registration tests. The results of the rigid registrations for the patient-based phantoms are shown in Table 2. The registration algorithm was successful for 47.9% of the tests across all phantoms.

3.1.2. Groupwise registration

The registration was performed on vertebrae L2, L3 and L4 and the US volume was cropped to correspond, as seen in Fig. 7. Registration is performed simultaneously for all three vertebrae, producing an 18-parameter optimization loop (3×6 rigid parameters). The middle vertebrae were chosen for the registration as they contained overlap from other vertebrae at the facet joints. This produces more realistic images in US and CT than including L1 and L5, as in our phantoms they have no overlap on their outer articular processes. Similar to the rigid registration, the CT volume was initially misaligned to a range of 0–20 mm TRE. Each vertebra was then further misaligned by individually applying a random transformation using a uniform distribution of ±5 mm translation along each axis and ±5° rotation about each axis. This transformation is not constrained to disallow collisions between vertebrae. While this misalignment is larger than what would be seen in a realistic situation, we chose this distribution to ensure that the registration capture range is greater than that of a clinical setting. The registrations were repeated for σ values of 0, 0.5, 1 and 2, representing the weight of the biomechanical model relative to the LC^2 similarity metric (Eq. (12)).

Table 2
Final TRE for the rigidly registered CT volumes from the patient-based phantoms, after individual vertebra were perturbed, are presented for vertebrae L2–L4 for all successful registrations. The initial TRE is reported for the successful registration with the largest mean initial error across all three vertebrae. Success rate (SR) is defined as the percentage of registrations where all vertebrae have a final TRE of less than 3 mm.

Phantom	L2 (mm/std)	L3 (mm/std)	L4 (mm/std)	Max iTRE (mm)	SR (%)
1	1.49/0.50	1.57/0.60	1.30/0.50	13.64	45.0
2	1.55/0.51	1.63/0.63	1.58/0.58	12.55	48.0
3	1.66/0.48	1.65/0.63	1.46/0.59	13.83	55.0
4	1.75/0.44	1.86/0.52	1.95/0.41	12.37	44.0
5	1.46/0.44	1.82/0.57	1.91/0.45	12.84	47.0

Similar to the rigid registration, TRE is calculated from the errors of the corners of the bounding box for each vertebra after registration. A registration is considered failed if any of the three vertebrae have a final TRE greater than the maximum clinically acceptable error of 3 mm.

Results for the groupwise registration tests on the patient-based phantoms are found in Table 3. The success rate across all the phantoms was 96.4%. The success rate for the phantom data was highest with a σ value of 1, an equal weighting of the biomechanical model and the intensity-based LC^2 metric. An example of the initial misalignment and the final registration is displayed in Fig. 8, where CT contours are overlaid on to US slices extracted along the principal axes. A demonstration of the effect of the rigid initialization is shown in Fig. 9, with sagittal slices from US overlaid with CT contours showing alignment prior to registration, after the rigid registration initialization and after the groupwise registration. As can been seen, the rigid registration brings the CT volume closer to the correct alignment, but

Table 3
Final TRE for vertebrae L2–L4 of the patient-based phantoms are presented for all successful groupwise registration. The initial TRE is reported for the successful registration with the largest mean initial error across all three vertebrae. Success rate (SR) is defined as the percentage of registrations where all the vertebrae have a final TRE of less than 3 mm.

Phantom	σ	L2 (mm/std)	L3 (mm/std)	L4 (mm/std)	Max iTRE (mm)	SR (%)
1	0.0	1.83/0.66	1.68/1.34	1.15/0.34	16.78	64.0
	0.5	1.95/0.68	1.46/0.52	1.06/0.22	18.76	86.0
	1.0	1.56/0.34	0.90/0.24	0.95/0.24	19.22	95.0
	2.0	1.66/0.30	1.77/0.22	0.91/0.13	19.22	93.0
2	0.0	1.74/0.25	1.19/0.21	2.41/1.62	14.63	57.0
	0.5	1.68/0.19	1.20/0.36	2.22/0.81	18.67	89.0
	1.0	1.61/0.17	1.32/0.35	1.56/0.41	19.31	98.0
	2.0	1.66/0.27	1.36/0.33	1.67/0.47	18.82	94.0
3	0.0	2.03/0.42	0.88/0.11	2.48/1.19	14.35	63.0
	0.5	1.88/0.31	0.83/0.09	2.15/1.08	18.28	84.0
	1.0	1.76/0.25	0.79/0.10	1.52/0.37	19.45	98.0
	2.0	1.65/0.29	0.83/0.08	1.55/0.70	19.45	94.0
4	0.0	2.32/0.51	1.73/0.43	2.25/0.48	17.84	81.0
	0.5	2.15/0.43	1.81/0.30	2.05/0.16	19.33	96.0
	1.0	1.96/0.32	1.92/0.27	2.01/0.12	19.33	98.0
	2.0	1.83/0.23	2.03/0.27	2.14/0.11	19.33	96.0
5	0.0	1.56/0.34	1.98/0.71	2.70/0.91	15.85	60.0
	0.5	1.50/0.30	2.53/0.32	2.06/0.33	18.25	90.0
	1.0	1.49/0.26	2.59/0.30	2.03/0.18	18.43	93.0
	2.0	1.45/0.22	2.49/0.18	2.05/0.16	18.25	91.0

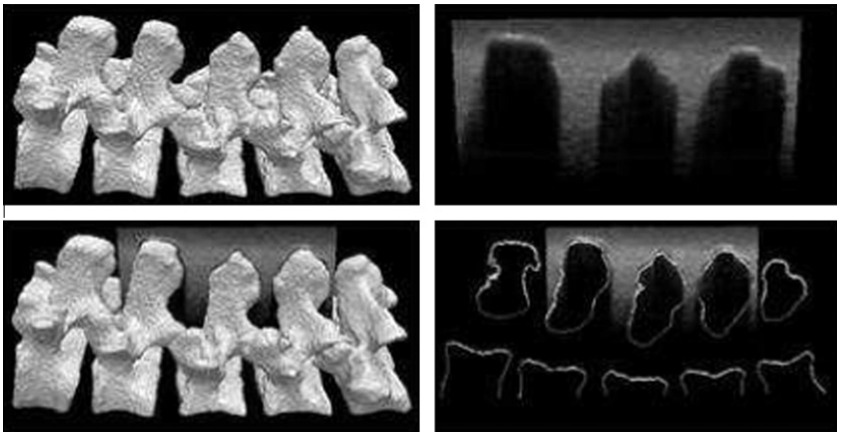

Fig. 7. Surface model of L1 to L5 (top left); US slice of L2 to L4 (top right). Overlaid US with surface model (bottom left) and corresponding extracted slice (bottom right).

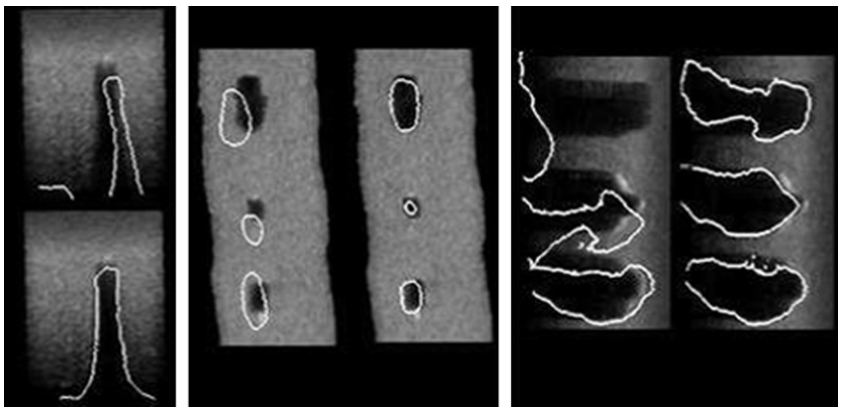

Fig. 8. Transverse (left), Coronal (center) and Sagittal (right) slices of the US volume from patient-based phantom 2 overlaid with the bone contours in the misaligned CT volumes and in the registered CT volumes. The transverse slice is taken from L3, the vertebra found in the middle of the coronal and sagittal slices.

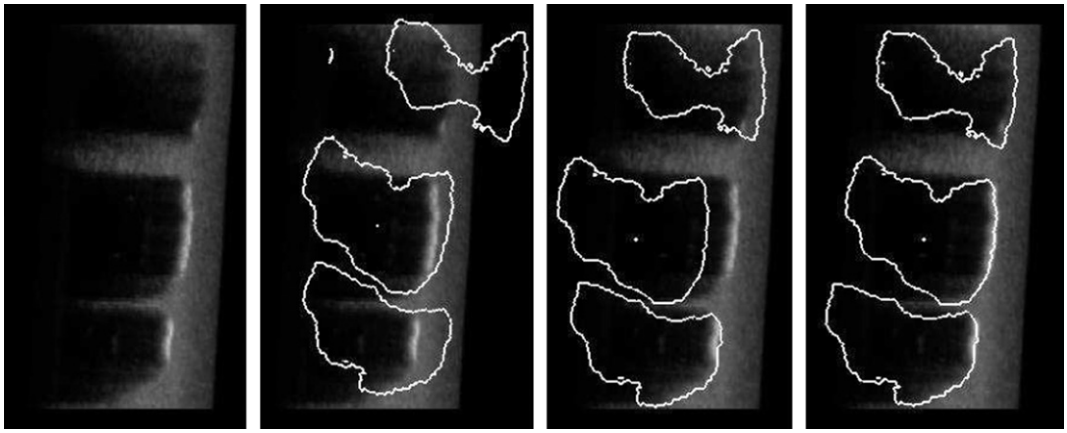

Fig. 9. Sagittal US slice from patient-based phantom 1 (left), with CT contours overlaid before registration (center left), after the rigid registration initialization (center right) and after the groupwise registration (right).

the groupwise registration results in alignments that could not be achieved with a strictly rigid registration.

3.2. Curved phantom registration

For a sixth patient-based phantom, US and CT data were collected twice: once with the model retaining the natural curvature of the spine and once introducing an approximately 4° curvature between the vertebrae, along the transverse axis. The difference between the two datasets are shown in Fig. 10.

The groupwise registration was tested by registering the natural phantom CT to curved phantom US. This was done to more accurately mimic the difference that will be observed in clinical data, where the curve in the anatomy will not match across US and CT. After initially aligning the datasets using a rigid registration, the CT volume was initially misaligned to a range of 0–20 mm. Unlike the previous groupwise tests, no additional displacement of the vertebrae was introduced. To measure the accuracy of this registration, four fiducial markers that are visible in CT were attached to the vertebral bodies. The fiducial markers were placed so that they would not be directly visible in the US images. The gold standard was calculated by registering each vertebra based on the fiducials visible in CT. For example, the gold standard alignment for L2 in the natural CT and curved US datasets is calculated by aligning

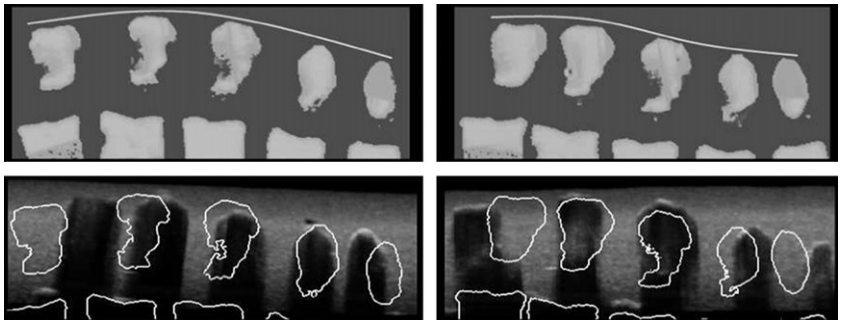

Fig. 10. Sagittal slices of the natural curved patient-based spine phantom (right) and of the increased curved patient-based phantom (left).

the fiducials on the L2 vertebra in the natural CT and the curved CT. Error is reported as the TRE of the corners of each vertebrae subvolume. Similar to the previous tests, a registration is considered failed if any of the three vertebrae have a final TRE of greater than the maximum clinically acceptable error of 3 mm. The results of the registration of the curved phantom are reported in Table 4. For these cases, rigid registration alone was unable to successfully register the datasets. Across the registrations in both directions (curved/natural, natural/curved), the algorithm had a success rate of 98.5%. The highest success rate for the registration of the curved phantom CT to the natural phantom US was with a σ value of 1, while the registration of the natural phantom CT to the curved phantom US was most successful with σ values of both 0.5 and 1.

3.3. Sheep cadaver

A similar approach for determining the gold standard was used for the sheep cadaver data. Ten fiducial markers used for calculating the gold standard were placed on the skin surface. The positions of these markers were determined manually in the CT, and using a tracked stylus to identify the tip of each fiducial in the US space. The entire lumbar spine, L1–L6, was imaged in both US and CT.

3.3.1. Rigid registration

The rigid registration was validated using a similar method to the patient-based phantom tests. The registration was performed on vertebrae L3, L4 and L5. We omitted L6 from the cadaver as there was significant overlap with the sacrum which produced different images than those that would be found in human data. One hundred registrations of the CT and US data were performed on the data with initial TRE ranging from 0 mm to 20 mm. The CT and US volumes were aligned using the fiducial-based gold standard transform and the CT volume was then misaligned by a random transformation chosen from a uniform distribution of ±10 mm translation along each axis and ±10° rotation about each axis. The misaligned CT volumes were then registered back to the US volume using our US simulation-based registration algorithm. Accuracy was determined by the ability of the registration to recover to the gold standard alignment and is reported as the mean TRE calculated as the RMS misalignment of the eight corners of the volume. The registration algorithm was successful for 99% of tests, with a mean TRE of 1.25 mm in the successful cases and a standard deviation of 0.14 mm. An example of an initial misalignment and final registration is presented in Fig. 11.

Similar to the patient-based phantom tests, we performed an additional 100 rigid registrations, where prior to registration the vertebrae were perturbed in CT to produce a different alignment than that found in US. Each vertebra was misaligned by individually applying a random transform using a uniform distribution of ±5 mm translation along each axis and ±5° rotation about each axis. The volumes were then reconstructed, filling in any gaps with a simulated soft-tissue value. This CT volume was then misaligned by the same set of transformations used in the previous rigid registration tests. The results of the rigid registrations for the sheep cadaver is shown in Table 5. The registration algorithm was successful for 32% of misalignments.

3.3.2. Groupwise registration

Validation of the groupwise registration was performed similarly to the method used for the patient-based phantoms. The registration was performed on vertebrae L3, L4 and L5 and the US volume was cropped accordingly. Registration was performed simultaneously for all three vertebrae, producing an 18-parameter optimization loop (3×6 rigid parameters). Similar to the rigid registration experiment, the CT volume was initially misaligned to a range of 0–20 mm TRE. Each vertebra was then further misaligned by individually applying a random transformation using a uniform distribution of 5 mm translation along each axis and 5° rotation about each axis. Results for the groupwise registration tests on the sheep cadaver are found in Table 6. The maximum success rate

Table 4
Final TRE for vertebrae L2–L4 of the curved patient-based phantom are presented for all successful registrations. The initial TRE is reported for the successful registration with the largest mean initial error across all three vertebrae. Success rate (SR) is defined as the percentage of registrations where all the vertebrae have a final TRE of less than 3 mm. In this table, Natural CT signifies the CT acquired from the natural phantom and Curved US signifies the US acquired from the curved phantom.

CT–US	σ	L2 (mm/std)	L3 (mm/std)	L4 (mm/std)	Max iTRE (mm)	SR (%)
Natural–curved	0.0	1.50/0.20	1.24/0.14	1.49/0.20	18.63	87
	0.5	1.46/0.16	1.11/0.24	1.46/0.17	19.54	100
	1.0	1.42/0.19	0.97/0.22	1.57/0.22	19.54	100
	2.0	1.38/0.19	0.94/0.22	1.90/0.28	19.54	98
Curved–natural	0.0	1.96/0.26	2.00/0.17	2.34/0.49	11.24	52
	0.5	1.97/0.13	1.95/0.09	2.27/0.31	18.36	92
	1.0	2.03/0.13	2.02/0.09	2.33/0.26	19.47	97
	2.0	2.07/0.10	2.13/0.06	2.42/0.24	19.47	95

Table 5
Final TRE for the rigidly registered CT volumes from the sheep cadaver, after individual vertebra were perturbed, are presented for vertebrae L3–L5 for all successful registrations. The initial TRE is reported for the successful registration with the largest mean initial error across all three vertebrae. Success rate (SR) is defined as the percentage of registrations where all the vertebrae have a final TRE of less than 3 mm.

	L3 (mm/std)	L4 (mm/std)	L5 (mm/std)	Max iTRE (mm)	SR (%)
Sheep	1.67/0.18	1.66/0.17	1.72/0.17	19.44	95
Sheep (misaligned)	2.03/0.41	2.07/0.42	2.00/0.47	8.53	32

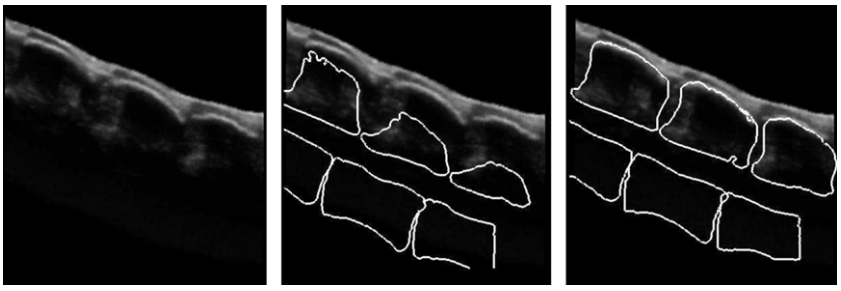

Fig. 11. Sagittal US slice from the sheep cadaver (left), overlaid with bone contours from the initially misaligned CT volume (center) and registered CT volume (right). Vertebrae in these images from left to right are L3, L4 and L5.

Table 6
Final TRE for vertebrae L3–L5 of the sheep cadaver are presented for all successful registrations. The initial TRE is reported for the successful registration with the largest mean initial error across all three vertebrae. Success rate (SR) is defined as the percentage of registrations where all the vertebrae have a final TRE of less than 3 mm.

σ	L3 (mm/std)	L4 (mm/std)	L5 (mm/std)	Max iTRE (mm)	SR (%)
0.0	1.71/0.76	0.72/0.30	2.26/1.10	15.36	66
0.5	1.70/0.79	0.62/0.27	1.81/0.71	18.84	87
1.0	1.33/0.44	1.09/0.23	1.94/0.67	18.84	84
2.0	1.44/0.38	1.59/0.27	2.00/0.56	18.84	84

for the sheep cadaver data was 87% with a σ value of 0.5. An example of the initial misalignment and the final registration is displayed in Fig. 12.

4. Discussion

We tested various σ values for weighting the biomechanical model in order to determine how much emphasis should be placed on the model when compared to the LC^2 metric. If the weight of the model is too low, it will have limited impact, however if it is weighted too high, it will not allow for the accurate registration of anatomy that lie outside the model's expected orientation. In our tests on patient-based phantoms, we found that an equal weighting of the model and intensity metric produced the best results. The benefits of this biomechanical constraint are clearly tied to how closely the model estimates the actual pose of the spine and how flexible the model is in allowing the registration of anatomies that differ from the expected alignment. We have shown that this particular model was able to successfully register the CT and US from a curved patient-based phantom. The anatomy in the curved version of the phantom differs from the expected orientation of the vertebrae, but was still reliably registered. Still, it is possible that if the patient anatomy differs substantially from the biomechanical model's expected alignment, the model could prove a hindrance rather than a benefit. It should be noted that the biomechanical model employed was not designed for use in image registration. As such, it is possible that the model could be further optimized for this purpose. Additionally, the model should be studied to determine its accuracy for representing the changes in curvature seen in a clinical setting.

The registration of the natural phantom CT to the curved phantom US produced significantly more robust results than in our other patient-based phantom tests. Additionally, both a σ value of 0.5 and 1 produced the best results for this dataset, where as for all the other phantom tests the best results were only from a σ value of 1. It is possible that in the introduction of the curve, the overlapping articular processes on the vertebrae became more defined in the US volume. This in turn would make it easier for the intensity-based similarity metric to correctly identify the proper alignment of the vertebrae, resulting in improved success rate of the unconstrained groupwise registration. With regards to the high success rates for σ values of both 0.5 and 1, both would have benefited from an improved registration using the intensity-based metric. In addition, as the curved phantom US does not match the biomechanical model's expected orientation to the same degree as the unmodified patient-based phantoms, it is logical that a reduced weight to the model would produce better results. We still see a similar trend in that if too much weight is placed on the biomechanical model, in this case a σ value of 2, the proportion of successful registrations will decrease. The set of tests with the inverse set of data, registering the curved phantom CT to the natural phantom US, were performed to confirm this hypothesis. These results, presented in Table 4, were similar to those of the previous phantom tests and support our hypothesis explaining the improved accuracy in our natural phantom CT and curved phantom US registrations.

It is worth noting that our biomechanically constrained registration does not explicitly disallow collisions between vertebrae. We believe that the biomechanical model is sufficiently robust that, in combination with our intensity-based metric, such collisions will not occur. In our results, none of the registrations identified as successful contained collisions between vertebrae.

Additionally, a comparison of similarity metrics must be performed. Wein et al. (2008) presents a comparison of the LC^2 similarity metric with MI, CR and higher-dimensional MI. While LC^2 was found to be the most robust and accurate, given the changes made to the US simulation in our algorithm, we may need to revisit the optimality of this metric in a clinical setting.

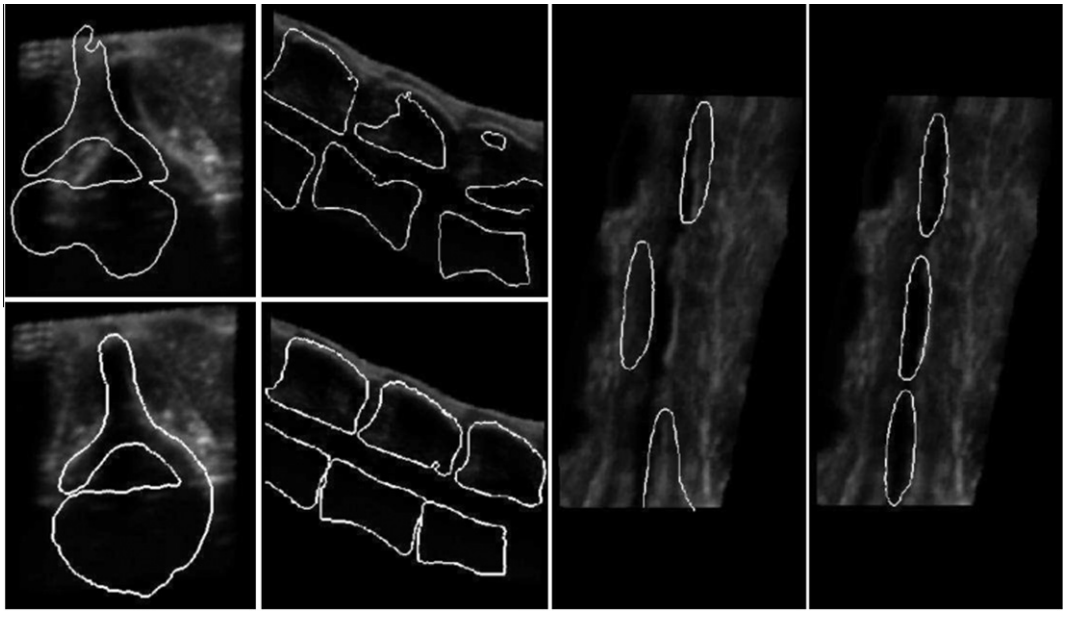

Fig. 12. Transverse (left), Sagittal (center,) and Coronal (right) slices of the US volume from the sheep cadaver, overlaid with the bone contours in the misaligned CT volumes and in the registered CT volumes. The transverse slice is taken from the center vertebra L4 (top).

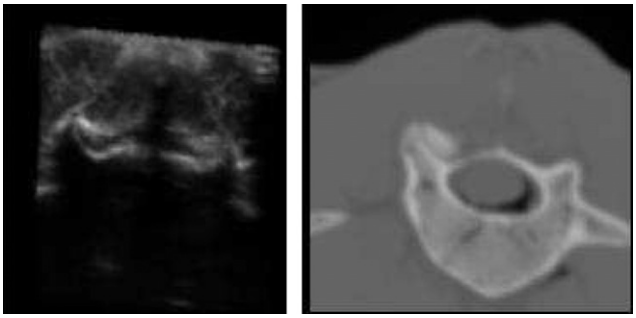

Fig. 13. A slice from the US volume (Left) and the corresponding CT slice (right) from the sheep cadaver. Strong reflections corresponding to the bone surface can be on the left side of the US slice.

One result of note is that for the sheep cadaver data, the registration was the most robust with a σ value of 0.5. This is likely due to the fact that the model is based on human data and is not an accurate of a representation of the sheep anatomy. In particular, the scale difference between the sheep vertebrae and human vertebrae likely made the biomechanical model stricter in the sheep data, thus requiring a lower σ value than the registrations for human data.

The registration algorithm proved to be robust to noisy and non-ideal data. As can be seen in Fig. 13, in the sheep cadaver, the US signal passed through the vertebra. Strong reflections are visible on the top and bottom of the bone, as well as the bone surface found below the superior articular process. This occurred several times throughout our US data and the algorithm was still able to successfully register both datasets.

Through the simultaneous registration of all three vertebrae in our groupwise registration, we are able to eliminate the chance of propagating error that can occur with consecutive registrations of vertebrae. This introduces a challenge to the registration as the 18 simultaneous parameters are more difficult to optimize than three independent sets of six parameters. Particularly, when all three vertebrae are fairly close to the appropriate alignment, changes in the alignment of one vertebra have a small impact on the similarity metric value. This is an implicit challenge of distilling 18 parameters representing three independent bodies into a single similarity metric. The inclusion of the biomechanical model aids in this issue and helps the algorithm converge faster, however it is necessary to have very strict convergence criteria.

5. Conclusion

We presented an US to CT registration technique for the lumbar spine. The algorithm was validated on a sheep cadaver and patient-based phantoms that were faithful in representing a realistic curvature of the spine. All registrations began with an initial misalignment between 0 mm and 20 mm. The groupwise registration algorithm applied iterative US simulation from CT images while allowing independent motion of each vertebra. A biomechanical model was introduced to represent the intervertebral interfaces and the system energy was calculated based on the relative transforms between the vertebrae. Integration of a biomechanical model to constrain the registration greatly improved the consistency of the algorithm. For the patient-based phantoms, 98.8% of rigid registrations were successful. Only 47.9% of tests with perturbed vertebrae were successfully registered with the rigid registration, while the groupwise registration, with a σ biomechanical model weight of 1, achieved a clinically acceptable registration for 95% of the tests. For the patient-based phantom with the introduced curvature between imaging acquisitions, rigid registration was unable to successfully register the datasets. The groupwise registrations of the curved phantom CT to the natural phantom US were successful for 97% of tests with a σ value of 1. Tests for registering the natural phantom CT to the curved phantom US had a success rate of 100% for σ values of 0.5 and 1. For the sheep cadaver data, 99% of rigid registrations for matching data were successful. For perturbed vertebrae, 35% of the rigidly registered datasets were successful and 87% of groupwise registrations were successful. For this case, the σ value for the biomechanical model was set to 0.5. These results show that our US to CT registration technique can accurately and reliably register images of the lumbar spine, regardless of changes in curvature between the preoperative and intraoperative imaging.

As future work, we will verify the proposed registration algorithm on human cadaver data. This would allow us to test our registration technique on clinically realistic data, including deformation of soft tissue between the preoperative and intraoperative imaging. For our algorithm to be practical in a clinical setting, the registration runtime must be decreased. The mean groupwise registration runtime across all phantom datasets with the C++/Insight Tool Kit (ITK) implementation was 43 min. In our preliminary tests of a GPU implementation, the mean registration runtime was 4 min. We are currently developing an optimized implementation for GPU. Finally, we are in the process of developing an interventional interface that, using our US to CT registration, will guide needle placement for percutaneous spine interventions.

Acknowledgements

This work has been partially funded by NSERC and CIHR. Special thanks to A. Lang, K. Wang, S. Lyman, J. Lazazzera and M. Kunz for their help with data acquisition and preparation.

References

Allen, H., Hubbard, D., Sullivan, S., 2005. The burden of pain on employee health and productivity at a major provider of business services. Journal of Occupational and Environmental Medicine 47 (7), 658–670.

Amin, D.V., Kanade, T., DiGioia, A.M., Jaramaz, B., 2003. Ultrasound registration of the bone surface for surgical navigation. Computer Aided Surgery 8 (1), 1–16.

Barratt, D.C., Penney, G., Chan, C.S., Slomczykowski, M., Carter, T.J., Edwards, P.J., Hawkes, D.J., 2005. Self-calibrating ultrasound-to-CT bone registration. In: MICCAI 2005 Proceedings of Lecture Notes in Computer Science, vol. 3749. Springer, pp. 605–612.

Besl, P., McKay, H., 1992. A method for registration of 3-D shapes. IEEE Transactions on Pattern Analysis and Machine Intelligence 14 (2), 239–256.

Carrat, L., Tonetti, J., Merloz, P., Troccaza, J., 2000. Percutaneous computer assisted iliosacral screwing: clinical validation. In: MICCAI 2000 Proceedings of Lecture Notes in Computer Science, vol. 1935. Springer, pp. 1229–1237.

Chen, T.K., Thurston, A.D., Moghari, M.H., Ellis, R.E., Abolmaesumi, P., 2008. A real-time ultrasound calibration system with automatic accuracy control and incorporation of ultrasound section thickness. In: SPIE Medical Imaging 2008, vol. 6918, p. 69182A.

Desroches, G., Aubin, C.E., Sucato, D.J., Rivard, C.H., 2007. Simulation of an anterior spine instrumentation in adolescent idiopathic scoliosis in a flexible multi-body model. Medical and Biological Engineering and Computing 45 (8), 759–768.

Environics Research Group Limited, 2003. Survey of canadian adults: back pain. Tech. rep.

Galiano, K., Obwegeser, A.A., Bodner, G., Freund, M., Maurer, H., Kamelger, F.S., Schatzer, R., Ploner, F., 2005. Ultrasound guidance for facet joint injections in the lumbar spine: a computed tomography-controlled feasibility study. Anesthesia Analgesia 101 (2), 579–583.

Gardner-Morse, M.G., Laible, J.P., Stokes, I.A.F., 1990. Incorporation of spinal flexibility measurements into finite element analysis. Journal of Biomechanical Engineering 112, 481–483.

Gill, S., Mousavi, P., Fichtinger, G., Boisvert, J., Chen, E., Pichora, D., Abolmaesumi, P., 2009a. Biomechanically constrained groupwise US to CT registration of the lumbar spine. In: MICCAI 2009 Proceedings of Lecture Notes in Computer Science, vol. 5761. Springer, pp. 803–810.

Gill, S., Mousavi, P., Fichtinger, G., Pichora, D., Abolmaesumi, P., 2009b. Group-wise registration of ultrasound to CT images of human vertebrae. In: SPIE Medical Imaging 2009, p. 72611O.

Hansen, N., Mnller, S.D., Koumoutsakos, P., 2003. Reducing the time complexity of the derandomized evolution strategy with covariance matrix adaptation (CMA-ES). Evolutionary Computation 11 (1), 1–18.

Herring, J., Dawant, B., Maurer, C., Muratore, D., Galloway Jr., R., Fitzpatrick, J., 1998. Surface-based registration of CT images to physical space for image-guided surgery of the spine: a sensitivity study. IEEE Transactions on Medical Imaging 17 (5), 743–752.

Huang, X., Hill, N.A., Ren, J., Peters, T.M., 2006. Rapid registration of multimodal images using a reduced number of voxels. In: SPIE Medical Imaging 2006, p. 614116.

Jensen, J.A., 1996. Field: a program for simulating ultrasound systems. Medical and Biological Engineering and Computing 34, 351–353.

Jensen, J.A., Svendsen, N.B., 1992. Calculation of pressure fields from arbitrarily shaped, apodized, and excited ultrasound transducers. IEEE Transactions on Ultrasonics, Ferroelectrics, and Frequency Control 29, 262–267.

Kadoury, S., Paragios, N., 2009. Surface/volume-based articulated 3D spine inference through markov random fields. In: MICCAI 2009 Proceedings of Lecture Notes in Computer Science, vol. 5762. Springer, pp. 92–99.

Kutter, O., Karamalis, A., Wein, W., Navab, N., 2009. A GPU-based framework for simulation of medical ultrasound. In: SPIE Medical Imaging 2009, p. 726117.

Madsen, E.L., Hobson, M.A., Shi, H., Varghese, T., Frank, G.R., 2005. Tissue-mimicking agar/gelatin materials for use in heterogeneous elastography phantoms. Physics in Medicine and Biology 50 (23), 5597–5618.

Mahowald, M.L., Singh, J.A., Majeski, P., 2005. Opioid use by patients in an orthopedics spine clinic. Arthritis and Rheumatism 52 (1), 312–321.

Moghari, M.H., Abolmaesumi, P., 2005. A novel incremental technique for ultrasound to CT bone surface registration using unscented Kalman filtering. In: MICCAI 2005 Proceedings of Lecture Notes in Computer Science, vol. 3750. Springer, pp. 197–204.

Muratore, D.M., Russ, J.H., Dawant, B.M., Galloway Jr., R.L., 2002. Three-dimensional image registration of phantom vertebrae for image-guided surgery: a preliminary study. Computer Aided Surgery 7 (6), 342–352.

Panjabi, M., Brand, R., White, A., 1976. Mechanical properties of the human thoracic spine as shown by three-dimensional load–displacement curves. The Journal of Bone and Joint Surgery 58, 642–652.

Penney, G., Barratt, D., Chan, C., Slomczykowski, M., Carter, T., Edwards, P., Hawkes, D., 2006. Cadaver validation of intensity-based ultrasound to CT registration. Medical Image Analysis 10 (3), 385–395.

Raj, P., Lou, L., Erdine, S., Staats, P.S. (Eds.), 2003. Radiographic Imaging for Regional Anaesthesia and Pain Management. Churchill Livingstone, Elsevier Science, Philadelphia.

Reichl, T., Passenger, J., Acosta, O., Salvado, O., 2009. Ultrasound goes GPU: real-time simulation using CUDA. In: SPIE Medical Imaging 2009, p. 726116.

Shams, R., Hartley, R., Navab, N., 2008. Real-time simulation of medical ultrasound from CT images. In: MICCAI 2008 Proceedings of Lecture Notes in Computer Science, vol. 5242. Springer, pp. 734–741.

Shao, W., Wu, R., Ling, K.V., Thng, C.H., Ho, H.S.S., Cheng, C.W.S., Ng, W.S., 2006. Evaluation on similarity measures of a surface-to-image registration technique for ultrasound images. In: MICCAI 2006 Proceedings of Lecture Notes in Computer Science, vol. 4191. Springer, pp. 472–479.

Stewart, W.F., Ricci, J.A., Chee, E., Morganstein, D., Lipton, R., 2003. Lost productive time and cost due to common pain conditions in the US workforce. Journal of the American Medical Association 290 (18), 2443–2454.

Tonetti, J., Carrat, L., Blendea, S., Merloz, P., Troccaz, J., Lavallee, S., Chirossel, J.-P., 2001. Clinical results of percutaneous pelvic surgery. Computer assisted surgery using ultrasound compared to standard fluoroscopy. Computer Aided Surgery 6 (4), 204–211.

von Berg, J., Kruecker, J., Schulz, H., Meetz, K., Sabczynski, J., 2004. A hybrid method for registration of interventional CT and ultrasound images. In: CARS 2004, Proceedings of International Congress Series, vol. 1268, pp. 492–497.

Wein, W., Brunke, S., Khamene, A., Callstrom, M.R., Navab, N., 2008. Automatic CT-ultrasound registration for diagnostic imaging and image-guided intervention. Medical Image Analysis 12 (5), 577–585.

Wein, W., Khamene, A., Clevert, D.-A., Kutter, O., Navab, N., 2007. Simulation and fully automatic multimodal registration of medical ultrasound. In: MICCAI 2007 Proceedings of Lecture Notes in Computer Science, vol. 4791. Springer, pp. 136–143.

Wein, W., Roper, B., Navab, N., 2005. Automatic registration and fusion of ultrasound with CT for radiotherapy. In: MICCAI 2005 Proceedings of Lecture Notes in Computer Science, vol. 3750. Springer, pp. 303–311.

Wilke, H.-J., Kettler, A., Wenger, K.H., Claes, L.E., 1997. Anatomy of the sheep spine and its comparison to the human spine. The Anatomical Record 247 (4), 542–555.

Winter, S., Brendel, B., Pechlivanis, I., Schmieder, K., Igel, C., 2008. Registration of CT and intraoperative 3-D ultrasound images of the spine using evolutionary and gradient-based methods. IEEE Transactions on Evolutionary Computation 12 (3), 284–296.